

In vivo two-photon imaging of mouse hippocampal neurons in dentate gyrus using a light source based on a high-peak power gain-switched laser diode

Ryosuke Kawakami,^{1,2,5,6} Kazuaki Sawada,^{1,2,6} Yuta Kusama,³ Yi-Cheng Fang,³ Shinya Kanazawa,⁴ Yuichi Kozawa,^{4,5} Shunichi Sato,^{4,5} Hiroyuki Yokoyama,^{3,5} and Tomomi Nemoto^{1,2,5,*}

¹ Research Institute for Electronic Science, Hokkaido University, Kita 20 Nishi 10, Kita-ku, Sapporo, 001-0020, Japan

² Graduate school of information science and technology, Hokkaido University, Kita 20 Nishi 10, Kita-ku, Sapporo, 001-0020, Japan

³ New Industry Creation Hatchery Center (NICHe), Tohoku University, 6-6-10 Aramaki-Aoba, Aoba-ku, Sendai, 980-8579, Japan

⁴ Institute of Multidisciplinary Research for Advanced Materials, Tohoku University, Katahira 2-1-1, Aoba-ku, Sendai, 980-8577, Japan

⁵ Core Research for Evolutional Science and Technology (CREST), Japan Science and Technology Agency (JST), Tokyo, Japan

⁶ These authors contributed equally to this work.

*tn@es.hokudai.ac.jp

Abstract: *In vivo* two-photon microscopy is an advantageous technique for observing the mouse brain at high resolution. In this study, we developed a two-photon microscopy method that uses a 1064-nm gain-switched laser diode-based light source with average power above 4 W, pulse width of 7.5-picosecond, repetition rate of 10-MHz, and a high-sensitivity photomultiplier tube. Using this newly developed two-photon microscope for *in vivo* imaging, we were able to successfully image hippocampal neurons in the dentate gyrus and obtain panoramic views of CA1 pyramidal neurons and cerebral cortex, regardless of age of the mouse. Fine dendrites in hippocampal CA1 could be imaged with a high peak-signal-to-background ratio that could not be achieved by titanium sapphire laser excitation. Finally, our system achieved multicolor imaging with neurons and blood vessels in the hippocampal region *in vivo*. These results indicate that our two-photon microscopy system is suitable for investigations of various neural functions, including the morphological changes undergone by neurons during physiological phenomena.

©2015 Optical Society of America

OCIS codes: (180.0180) Microscopy; (180.4315) Nonlinear microscopy; (180.2520) Fluorescence microscopy; (110.6880) Three-dimensional image acquisition.

References and links

1. Y. Masamizu, Y. R. Tanaka, Y. H. Tanaka, R. Hira, F. Ohkubo, K. Kitamura, Y. Isomura, T. Okada, and M. Matsuzaki, "Two distinct layer-specific dynamics of cortical ensembles during learning of a motor task," *Nat. Neurosci.* **17**(7), 987–994 (2014).
2. T. Matsui and K. Ohki, "Target dependence of orientation and direction selectivity of corticocortical projection neurons in the mouse V1," *Front. Neural Circuits* **7**, 143 (2013).
3. J. Lecoq, J. Savall, D. Vučinić, B. F. Grewe, H. Kim, J. Z. Li, L. J. Kitch, and M. J. Schnitzer, "Visualizing mammalian brain area interactions by dual-axis two-photon calcium imaging," *Nat. Neurosci.* **17**(12), 1825–1829 (2014).
4. J. Grutzendler, N. Kasthuri, and W. B. Gan, "Long-term dendritic spine stability in the adult cortex," *Nature* **420**(6917), 812–816 (2002).

5. M. Matsuzaki, N. Honkura, G. C. Ellis-Davies, and H. Kasai, "Structural basis of long-term potentiation in single dendritic spines," *Nature* **429**(6993), 761–766 (2004).
6. T. Nakashiba, J. D. Cushman, K. A. Pelkey, S. Renaudineau, D. L. Buhl, T. J. McHugh, V. Rodriguez Barrera, R. Chittajallu, K. S. Iwamoto, C. J. McBain, M. S. Fanselow, and S. Tonegawa, "Young dentate granule cells mediate pattern separation, whereas old granule cells facilitate pattern completion," *Cell* **149**(1), 188–201 (2012).
7. T. Nemoto, "Living cell functions and morphology revealed by two-photon microscopy in intact neural and secretory organs," *Mol. Cells* **26**(2), 113–120 (2008).
8. J. Noguchi, A. Nagaoka, S. Watanabe, G. C. Ellis-Davies, K. Kitamura, M. Kano, M. Matsuzaki, and H. Kasai, "*In vivo* two-photon uncaging of glutamate revealing the structure-function relationships of dendritic spines in the neocortex of adult mice," *J. Physiol.* **589**(10), 2447–2457 (2011).
9. W. Mittmann, D. J. Wallace, U. Czubayko, J. T. Herb, A. T. Schaefer, L. L. Looger, W. Denk, and J. N. D. Kerr, "Two-photon calcium imaging of evoked activity from L5 somatosensory neurons *in vivo*," *Nat. Neurosci.* **14**(8), 1089–1093 (2011).
10. M. Oheim, E. Beaufort, E. Chaigneau, J. Mertz, and S. Charpak, "Two-photon microscopy in brain tissue: parameters influencing the imaging depth," *J. Neurosci. Methods* **111**(1), 29–37 (2001).
11. R. Kawakami, K. Sawada, A. Sato, T. Hibi, Y. Kozawa, S. Sato, H. Yokoyama, and T. Nemoto, "Visualizing hippocampal neurons with *in vivo* two-photon microscopy using a 1030 nm picosecond pulse laser," *Sci. Rep.* **3**, 1014 (2013).
12. G. Feng, R. H. Mellor, M. Bernstein, C. Keller-Peck, Q. T. Nguyen, M. Wallace, J. M. Nerbonne, J. W. Lichtman, and J. R. Sanes, "Imaging neuronal subsets in transgenic mice expressing multiple spectral variants of GFP," *Neuron* **28**(1), 41–51 (2000).
13. Y. Kusama, Y. Tanushi, M. Yokoyama, R. Kawakami, T. Hibi, Y. Kozawa, T. Nemoto, S. Sato, and H. Yokoyama, "7-ps optical pulse generation from a 1064-nm gain-switched laser diode and its application for two-photon microscopy," *Opt. Express* **22**(5), 5746–5753 (2014).
14. A. Holtmaat, T. Bonhoeffer, D. K. Chow, J. Chuckowree, V. De Paola, S. B. Hofer, M. Hübener, T. Keck, G. Knott, W. C. Lee, R. Mostany, T. D. Mrsic-Flogel, E. Nedivi, C. Portera-Cailliau, K. Svoboda, J. T. Trachtenberg, and L. Wilbrecht, "Long-term, high-resolution imaging in the mouse neocortex through a chronic cranial window," *Nat. Protoc.* **4**(8), 1128–1144 (2009).
15. R. Mostany and C. Portera-Cailliau, "A craniotomy surgery procedure for chronic brain imaging," *J. Vis. Exp.* **12**(12), 3791 (2008).
16. W. Denk, J. H. Strickler, and W. W. Webb, "Two-photon laser scanning fluorescence microscopy," *Science* **248**(4951), 73–76 (1990).
17. J. Bewersdorf and S. W. Hell, "Picosecond pulsed two-photon imaging with repetition rates of 200 and 400 MHz," *J. Microsc. Oxford* **191**(1), 28–38 (1998).
18. H. Yokoyama, H. Guo, T. Yoda, K. Takashima, K. Sato, H. Taniguchi, and H. Ito, "Two-photon bioimaging with picosecond optical pulses from a semiconductor laser," *Opt. Express* **14**(8), 3467–3471 (2006).
19. K. König, T. W. Becker, P. Fischer, I. Riemann, and K. J. Halbhuber, "Pulse-length dependence of cellular response to intense near-infrared laser pulses in multiphoton microscopes," *Opt. Lett.* **24**(2), 113–115 (1999).
20. N. G. Horton, K. Wang, D. Kobat, C. G. Clark, F. W. Wise, C. B. Schaffer, and C. Xu, "In vivo three-photon microscopy of subcortical structures within an intact mouse brain," *Nat. Photonics* **7**(3), 205–209 (2013).
21. T. A. Murray and M. J. Levene, "Singlet gradient index lens for deep *in vivo* multiphoton microscopy," *J. Biomed. Opt.* **17**(2), 021106 (2012).

1. Introduction

Techniques capable of revealing the function and behavior of individual neurons in living tissues have the potential to provide a great deal of information about brain functions [1–3]. Recent advances have enabled non-invasive high-definition visualization of neural circuits in the living mouse brain using two-photon fluorescence microscopy [4–9]. However, the observation range of this method is limited to a depth of a few hundred micrometers from the surface of the brain. For live imaging by two-photon microscopy, mode-locked titanium-sapphire (Ti:Sa) lasers are frequently used as the excitation light source. The Ti:Sa laser, which is commercially available, has several advantages, including a variable output wavelength (690–1040 nm) and the ability to excite fluorescent materials. In order to penetrate organs, however, it is necessary to use longer wavelengths in the "biological window" between 900 and 1200-nm; consequently, the average power of the Ti:Sa lasers are not optimal for efficient tissue penetration. However, the details of the optical properties of individual organs are not completely known, and light transmittance is low even in near-infrared range in the brain [10]. In particular, less-invasive high-resolution observations and

analysis of neurons and synapses by *in vivo* two-photon microscopy have been performed successfully only in the cortical area of the mouse brain.

Therefore, in previous work we developed a novel high-peak power output laser with a 1030-nm 5-picosecond pulse width light source based on a mode-locked semiconductor, and evaluated the performance of this system in *in vivo* deep imaging of the Thy1-EYFP-H (H-line) transgenic mouse brain [11]. H-line mice express enhanced yellow fluorescent protein (EYFP) in a subset of the pyramidal neurons in layer V in cerebral cortex, CA1 pyramidal neurons, and dentate gyrus granule cells in the hippocampus [12]. As a result, we demonstrated *in vivo* imaging of young brain from the surface to the hippocampus until a depth of 1.4 mm. However, it was not possible to visualize the hippocampus in the adult mouse. This result indicated that high-peak power picosecond pulse laser is suitable for *in vivo* two-photon microscopy to investigate a deeper region of the young mouse brain. More recently, we newly developed a Gain-switched Semiconductor Laser Diode (GSLD) with a 1064-nm wavelength and 7.5-picosecond pulse width as a light source, and used this system to visualize cortical layer V pyramidal neurons in living brain [13].

In this study, we amplified this 1064-nm optical pulse using a high-output amplifier with Large Mode-Area (LMA) fiber, and introduced to upright laser scanning microscope that is commercially available from Nikon and is equipped with a GaAsP type Non-Descanned Detector (GaAsP-NDD) for high-sensitivity detection of visible fluorescence. To elucidate the performance of this system in *in vivo* imaging, we compared the penetration depths in the hippocampal regions achieved by a 1064-nm GSLD based light and a mode-locked Ti:Sa. Our newly developed two-photon microscopy enabled, for the first time, successful non-invasive *in vivo* observation of the hippocampal dentate gyrus granule cells at a depth of over 1.5 mm from the brain surface in both young and adult mice.

2. Materials and methods

2.1 Animals

Young adult (4 weeks-old) and adult (9 to 11 weeks-old) H-line mouse for *in vivo* imaging were used in this study. The expression pattern of EYFP in the H-line mouse enabled us to observe fluorescence signals from locations ranging from the hippocampus to the brain surface, and was therefore suitable for evaluating the penetration depth of two-photon microscopy. All mice were housed with food and water *ad libitum* on a 12:12 light-dark cycle (lights on from 08:00 to 20:00) with controlled temperature and humidity. The study was carried out in accordance with the recommendations in the Guidelines for the Care and Use of Laboratory Animals of the Animal Research Committee of Hokkaido University. All protocols were approved by the Institutional Animal Care and Use Committee of National University Corporation Hokkaido University (Permit Number: 10-0119).

2.2 Cranial window for *in vivo* two-photon imaging

For high-resolution imaging of synaptic structures in the cortex of living mice, the overlying opaque skull bone must be partially removed to make a cranial window, the “open-skull” glass window. In the open-skull preparation, a piece of the cranial bone (about 4 mm in diameter) is removed, leaving the dura intact, and the exposed brain is covered with a thin glass cover slip (for detailed methods, see published protocols [13–15]).

2.3 Excitation laser

A GSLD based light source with a wavelength of 1064-nm and a pulse width of 7.5- ps was operated at a 10-MHz repetition rate [13]. Each component was coupled in the optical fiber, and the final output was also made to the fiber output. The generated 1064-nm optical pulses

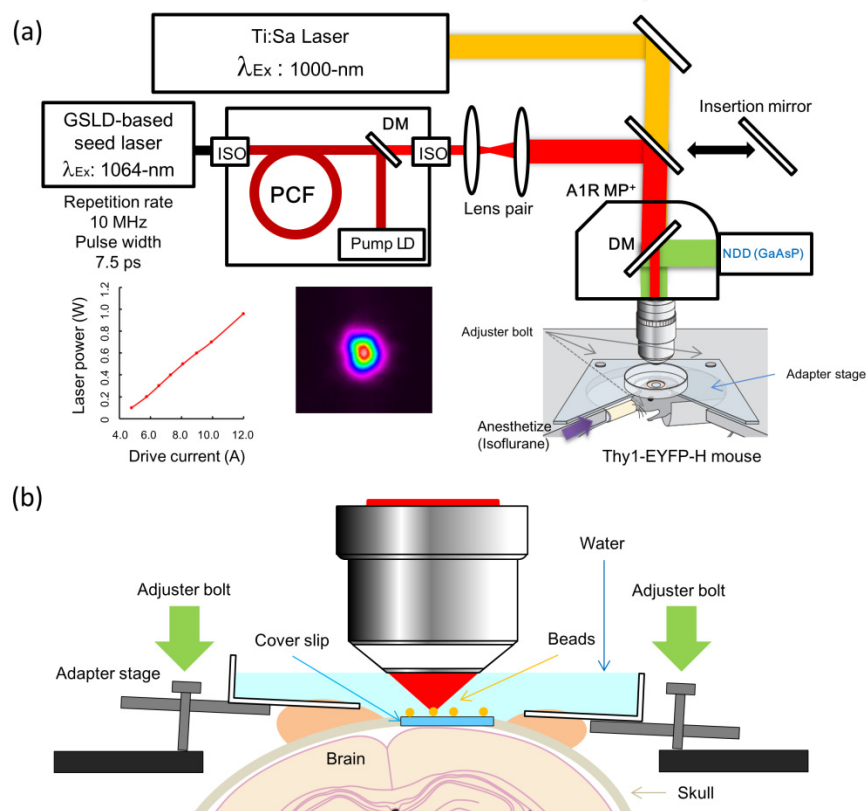


Fig. 1. Schematic diagram for *in vivo* two-photon microscopy using the novel GSLD based light source. (a) Optical arrangement for introduction of the 1064-nm picosecond (newly developed) GSLD-based seed laser and 1000-nm femtosecond (Ti:Sa) lasers into the two-photon microscope. The optical pathway from each laser is indicated by a red (GSLD) or orange (Ti:Sa) line. The pulse duration of the 1064-nm GSLD laser beam was about 7.5-picoseconds, and the average output power was over 4 W. The excitation laser was changed using an insertion mirror, and emissions were detected by GaAsP-NDD in the A1R MP⁺ (Nikon). Under the objective lens, the average excitation laser power was measured relative to the driver current of the pump LD for PCF. ISO: isolator, DM: dichroic mirror at 690-nm. A 35-mm disposable dish was mounted on the head of the H-line mouse. The mouse head was suspended from the adapter stage by the dish, and the body was held under the stage using a soft cloth. The apparatus included a horizontal adjustment mechanism to secure the head of the mouse under an upright microscope stage [11]. (b) Three adjuster bolts were located on the adapter stage. Fluorescent red beads were placed on the cover slip. The angle of adapter stage could be manually controlled using these bolts to ensure that the cover slip became horizontal observing these beads as an indicator of the cover slip angle.

were amplified by the Ytterbium doped fiber amplifier (YDFA) composed of a LMA photonic crystal fiber (PCF) (DC-200/40-PZ-Yb, NKT Photonics) with single-mode and polarization-maintaining characteristics. We used 915-nm laser diode (LD) as a pump LD for excitation of the PCF [Fig. 1(a)]. To control the final output power of the laser, we adjusted the driving current of the pump LD. In the case of *in vivo* imaging, we operated at a maximum power of 500-mW under the objective lens; at higher output powers, macroscopic failure in the cerebral cortex has been observed in many cases. In this report, we also used a MaiTai eHP DeepSee Ti:Sa laser (Spectra Physics) with variable wavelength. To compare the performance of the 1064-nm GSLD based light source, the Ti:Sa laser was operated at a wavelength of 1000-nm that could excite EYFP and provide steadily average output power. At first, we adjusted the laser power from 300 to 500 mW at a scanning speed of 1/32 fps for

positioning of the acquisition area and imaging of the dentate gyrus. Subsequently, we used a laser power from 200 to 300 mW and a scanning speed of 1/16 fps during imaging of the hippocampal CA1 region. After hippocampal imaging, we applied a power of 200 mW to the bottom of the cortex, and gradually decreased the power at a few mW and scanning speed by 1/4 or 1/8 fps as we approached the brain surface. For the Ti:Sa laser, during the imaging of the hippocampal region, laser power and scanning speed were set at 100 mW and 1/32 fps, respectively. In the cortical region, laser power gradually decreased to a few mW, and acquisition speed was set at 1/2 fps.

2.4 Image acquisition

Image stacks consisting of over 300 optical sections with 5- μm Z-steps were acquired from the deep region, an area covering $500 \times 500 \mu\text{m}$ (512×512 pixels, $0.994 \mu\text{m}/\text{pixel}$). These images were obtained using a two-photon laser microscope customized for *in vivo* imaging (A1R MP⁺, confocal microscope, Nikon) with a $25 \times$ water objective lens (NA 1.10). All of the fluorescence signals with wavelengths under 690-nm were detected via the GaAsP-NDD. The GaAsP-NDD was 2-fold more sensitive than a multi-alkali PMT in the visible region, and implemented 4-channel in the microscope. In the case of multicolor imaging of EYFP and Alexa Fluor 546, fluorescence was divided at a wavelength of 560 nm by a dichroic mirror in front of the GaAsP-NDD.

2.5 Data analysis

To calculate the signal peak-to-background ratio, all images under the alveus were analyzed using NIS element Ver.4.00 (Nikon). The depth of the alveus was defined as the position of the deepest alveus in each mouse. Before analysis, these images were filtered using 3×3 median filters. The signal-peak intensity of each individual image was measured from the maximum intensity of the 30- μm line profile (signal area of the pyramidal neuron; $n = 7$ each). The background intensity was calculated by averaging intensities of all pixels in 100- μm line profiles (non-signal area).

The signal peak-to-background ratio (R) was defined as follows:

$$R = I_s / \left(\sum_{i \in B.G.} I_b^i / N_b \right)$$

Here, I_s is the maximum fluorescence intensity in the line profile of the “signal” region. I_b^i is the fluorescence signal intensity of a single pixel, and N_b is the number of the pixels in the line profile of the background.

3. Results and discussion

We developed a GSLD that generates a 1064-nm wavelength with a 7.5-picosecond pulse width under strong excitation by high-intensity electrical pulse [13]. The 1064-nm GSLD-based seed laser was operated at a repetition rate of 10-MHz, and optical pulses were amplified by the LMA-YDFA to an average output power above 4 W. The M^2 value of the output laser beam was measured as 1.3. The amplified 1064-nm optical pulse was introduced to a two-photon microscope (A1R MP⁺, Nikon) equipped with a GaAsP-NDD. A mirror interrupted the optical path of the Ti:Sa laser the originally designed by Nikon, and the beam diameter was adjusted via a lens pair identical to that used for the Ti:Sa laser [Fig. 1(a)]. The maximum average laser power under the objective lens was above 1 W [Fig. 1(a)]. We examined the performance of our newly developed 1064-nm GSLD based light source in *in vivo* two-photon microscopy by observing the penetration depth in the H-line mouse brain. Following surgery to replace the skull with a cover glass, using the open-skull method, an H-line mouse was placed on the microscope stage with an adapter plate under inhalation anesthesia. The horizontal position of the cover slip on the brain differed between mice. Because tilting of the cover slip induced some aberrations and affected the imaging quality of

microscopic observations, we ensured the horizontality of the cover slip by optimizing the angle of the adapter stage [Fig. 1(b)].

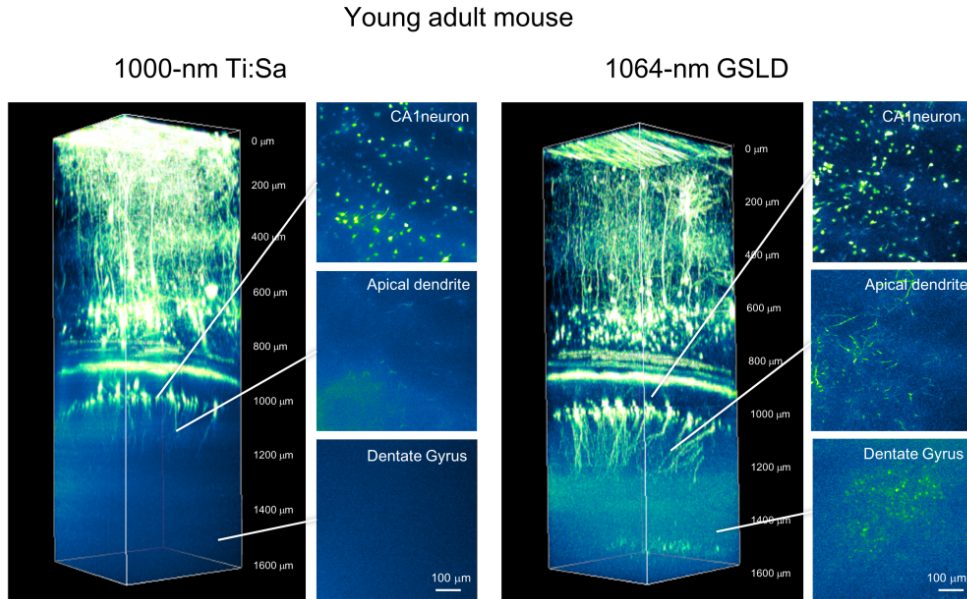


Fig. 2. Two-photon fluorescence imaging of cortical and hippocampal neurons with 1000-nm MaiTai eHP DeepSee and 1064-nm high-peak power GSLD based light-source excitation in young adult H-line mouse brain. Maximum intensity projections of three-dimensional stacks were obtained with a 1000-nm Ti:Sa laser (left panel) and a 1064-nm GSLD (right panel). Each xy image of the cortical region and hippocampal region was acquired under a different scanning condition. Six normalized xy frames from the z-stack at various depths are shown, including the hippocampal CA1 pyramidal cell layer, apical dendrites, and hippocampal dentate gyrus.

In young adult mice, we performed *in vivo* imaging using a Ti:Sa laser with a wavelength of 1000-nm. At that wavelength, the maximum incident power of the Ti:Sa laser under the objective lens was about 100 mW. The Ti:Sa laser with the GaAsP-NDD in the A1R MP⁺ visualized all layer V cortical neurons and hippocampal CA1 pyramidal neurons, including the white matter and hippocampal alveus. In the imaging of the cortical region, the 1064-nm GSLD based light successfully visualized the detailed structure of dendrites and fine processes. Surprisingly, the 1064-nm GSLD based light could visualize hippocampal CA1 pyramidal neurons, with fine structure of apical and basal dendrites, with a higher peak signal-to- background ratio. In addition, our system revealed granule cells in the dentate gyrus lying under the CA1 area [Figs. 2, 4].

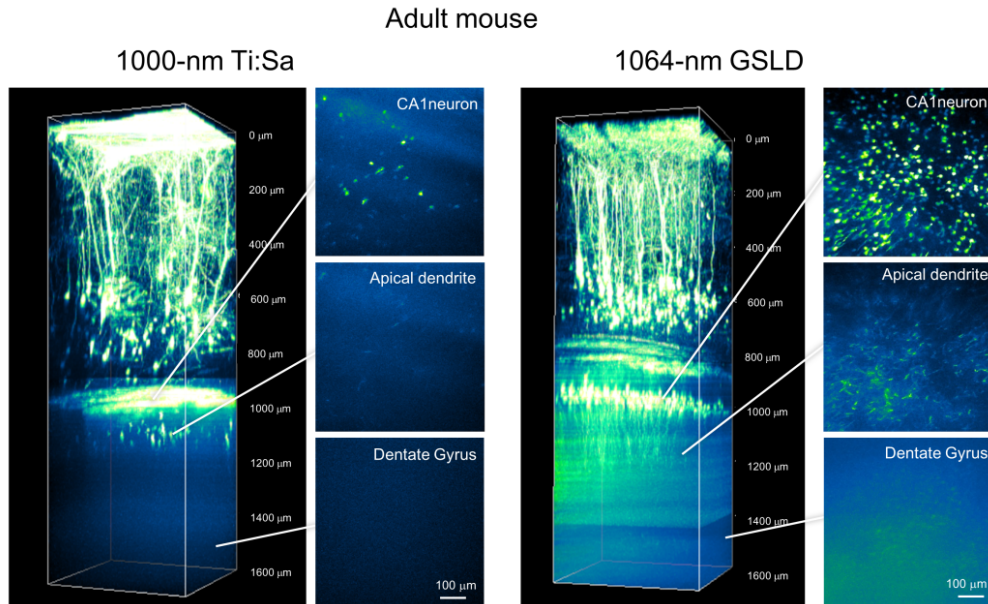


Fig. 3. Two-photon fluorescence imaging of cortical and hippocampal neurons with 1000-nm MaiTai eHP DeepSee and 1064-nm high-peak power GSLD based light source excitation in adult H-line mouse brain. Maximum intensity projections of three-dimensional stacks were obtained with the 1000-nm Ti:Sa laser (left panel) and 1064-nm GSLD (right panel). Each xy image of the cortical region and hippocampal region was acquired under different scanning conditions. Six normalized xy frames from the z-stack at various depths are shown, including the hippocampal CA1 pyramidal cell layer, apical dendrites, and hippocampal dentate gyrus.

Next, we examined the penetration depth in the adult mouse brain. Previously, *in vivo* imaging of the hippocampal region could barely be achieved in the adult mouse [11]. In the conventional system, using the Ti:Sa laser with the GaAsP-NDD, some hippocampal pyramidal neurons could be observed, but the tiny processes of basal and apical dendrites were not visible. On the other hand, the 1064-nm GSLD excitation revealed the entire cortical area and some of the neurons in the hippocampal CA1 area. In the most successful open-skull operations, in which no blood cell leaked onto the surface of the brain, we could identify granule cells at the dentate gyrus [Figs. 3, 4].

Next, we quantitatively analyzed the peak signal-to-background ratios of images of the hippocampal region. To distinguish a neural process in the xy-plane, the ratio between the signal intensity and the background was critical, especially in the deeper regions where fluorescence was dim. To avoid variation in the EYFP intensity as a result of morphological structure or fluctuations in the fluorescence image, we measured two intensities: (1) the “peak signal”, i.e., the peak intensity in lines containing a section of an identical neural process of a single neuron; and (2) the “background”, i.e., the average intensity in a neighboring line [Fig. 4; see also Materials and Methods]. We calculated peak signal-to-background ratios (R) among seven individual hippocampal neurons and plotted them in Fig. 4. These figures show that, both in young adult and adult mice, R decreased rapidly in layers deeper than 1100 μm when the Ti:Sa laser was used. By contrast, R was significantly higher, even at similar depths, when the 1064-nm GSLD based light source was used. Notably, for *in vivo* images of hippocampal neurons, we obtained higher R values with the 1064-nm GSLD based light source in layers deeper than 1.0 mm in both young adult and adult mice [Fig. 4].

Two-photon excitation allows redundancy, i.e., excitation of different fluorescent substances at the same time. Therefore, we injected red fluorescent dye (Alexa Fluor 546: 1.0 mg/ml in PBS, injection volume: 0.1 ml) into the bloodstream via the tail vein, and performed

multi-color imaging of neurons and blood vessels in the deep region of the H-line mouse brain. Using the 1064-nm GSLD based light source, we could visualize the blood vessel at the hippocampal fissure located between the dentate gyrus and hippocampus CA1 area [Fig. 5].

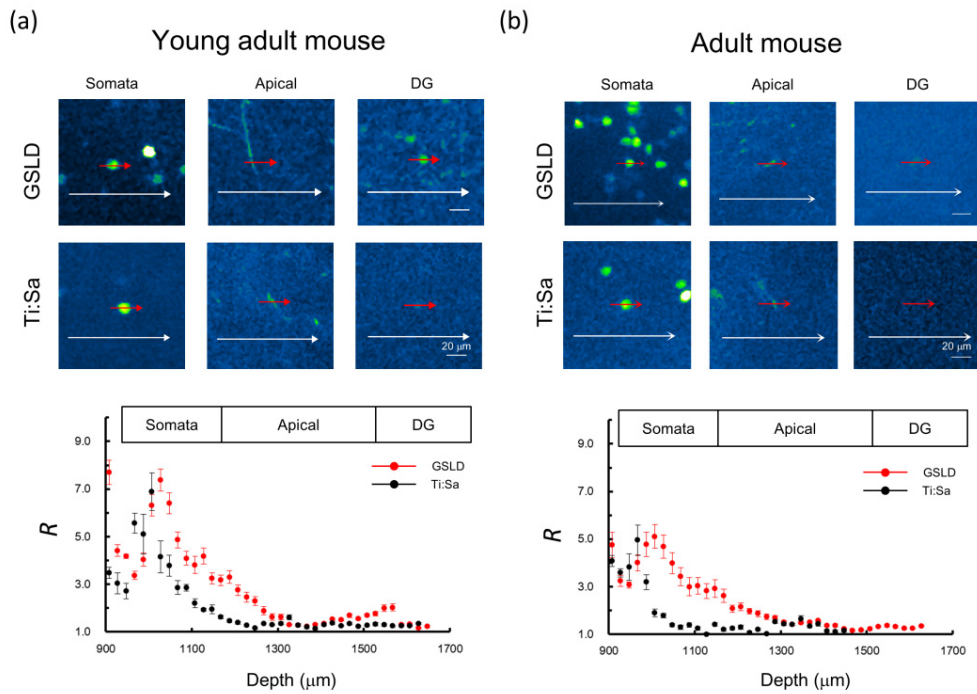


Fig. 4. Quantitative analyses of peak signal-to-background ratio for *in vivo* imaging of hippocampal neurons. (a) A cross-sectional (xy) image obtained from the hippocampal areas of young adult and adult mice. (b). In the upper panels, the signal and background peaks were calculated from fluorescence intensities in a line profile (20- μm diameter) across an individual neural process (signal: red line) and the background area (white line). The ratio R at each process was calculated by dividing the signal peak by the background (see Materials and Methods). The depth dependence of the average and Standard Error of the Mean of signal peak-to-background ratios (R) was calculated in young adult (a) and adult (b) mice. Red and black circles indicate averages obtained using the 1064-nm GSLD and 1000-nm Ti:Sa lasers, respectively ($n = 7$ processes; averages \pm SEM).

In this study, we achieved *in vivo* imaging of dentate gyrus granule cells at a depth of more than 1.5 mm from the brain surface and a panoramic view of the hippocampal CA1 pyramidal neurons in both young and adult mice, using a combination of a high-output picosecond 1064-nm GSLD based light source and the highly sensitive detector. In the hippocampal CA1 region, fine processes of the apical and basal dendrites could be visualized, even in the adult mouse; previously, the CA1 neurons could be observed by the 1030-nm laser only in young adult mice [11]. One of the reasons that fine processes of the pyramidal neurons could be observed with a high peak signal-to-background ratio was the higher output power of the 1064-nm GSLD based light source. The number of photons absorbed per fluorophore per second [16] under the objective lens was 13-fold higher than that obtained using a 1030-nm LD light source and 1.4-fold higher than that obtained using a 1000-nm Ti:Sa laser [Table 1]. This higher probability of absorption may be critical for revealing granule cells of the dentate gyrus in young adult mice. On the other hand, the 1000-nm Ti:Sa laser enabled visualization of adult mouse hippocampal pyramidal neurons, which was impossible in the case of the 910-nm Ti:Sa laser excitation used in previous work [11]. Compared with the previous case, the laser power under the objective lens was higher, and

the wavelength was longer. Furthermore, the high-sensitivity GaAsP-NDD detector effectively acquired signals from deeper region of the brain.

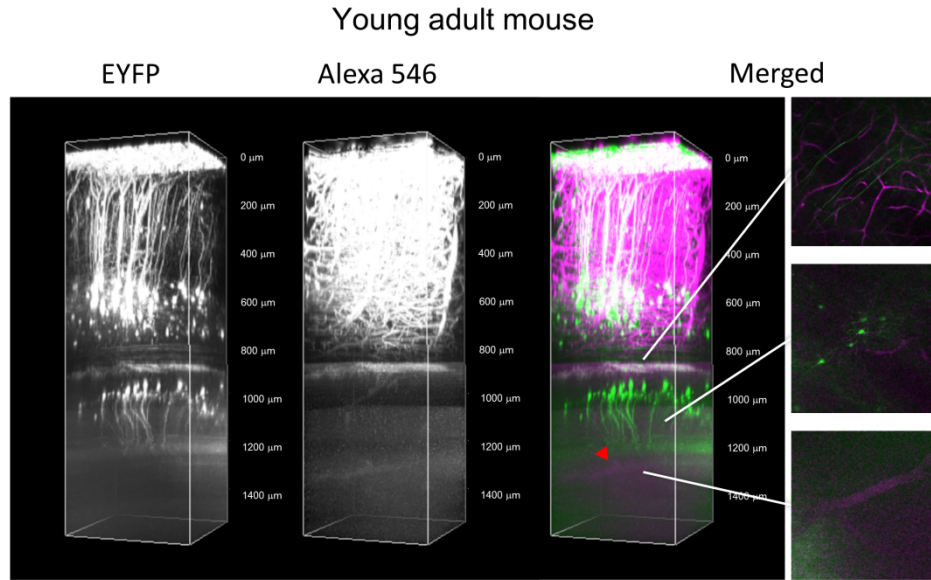


Fig. 5. *In vivo* multi-color imaging of EYFP in the pyramidal neurons and Alexa Fluor 546 in a blood vessel in the H-line mouse brain. Maximum intensity projections of three-dimensional stacks were obtained with the 1064-nm GSLD based light source. Each xy image was performed unmixing using NIS-ELEMENTS (Nikon) and excluding signals that overlapped with each other. Each stack contains EYFP and Alexa Fluor 546 signals. In the merged image, green and magenta indicate EYFP and Alexa Fluor 546, respectively. The cortical and hippocampal regions were acquired under different scanning conditions. Six normalized xy frames from the z-stack at various depths are shown, including the white matter, hippocampal CA1 pyramidal cell layer, and hippocampal fissure area. The red arrowhead indicates a large blood vessel relay on the hippocampus.

Table 1. Specifications of the 1064-nm GSLD based light, mode-locked Ti:Sa, and 1030-nm mode-locked LD based laser.

	λ_{ex}	τ_{pulse}	f_{repi}	P_{aver}	P_{peak}	Na
GSLD based laser	1064 nm	7.5 p sec	10 MHz	500 mW	6.7 kW	4.4×10^7
Mode-locked Ti:Sa laser	1000 nm	70 f sec	80 MHz	100 mW	17.9 kW	3.1×10^7
Mode-locked LD based laser	1030 nm	5.0 p sec	20 MHz	170 mW	1.7 kW	3.4×10^6

λ_{ex} : excitation wavelength. τ_{pulse} : pulse width. f_{repi} : repetition rate. P_{aver} : average power. P_{peak} : peak-power. Na : The number of photons absorbed per fluorophore per second [16].

Recently, a femtosecond light source from a Ti:Sa laser was applied to two-photon microscopy because it could achieve a high repetition rate with high fluorescence intensity. On the other hand, the Ti:Sa laser barely oscillates at the picosecond timescale. A picosecond pulse laser with a high repetition rate has been used to successfully excite fluorescent materials and achieve biological imaging [17]. In addition, a highly amplified picosecond pulse enabled us to visualize biological specimens and hippocampal neurons in the mouse brain *in vivo* [11,13,18]. Here, the number of photons absorbed per fluorophore per second Na [16] increases with the pulse width τ , the square of the peak power, and the repetition frequency as follows:

$$Na \propto P_{peak}^2 \tau_{pulse} f_{repi}$$

Therefore, even with long pulse widths (up to a few picoseconds), we can improve the two-photon fluorescence intensity by decreasing the pulse repetition rate and amplifying the picosecond pulse by using a PCF to 6.7 kW under the objective lens. Here, the peak-power of

the laser is represented as $P_{peak} = \frac{P_{average}}{\tau_{pulse} f_{repi}}$, then Na is rewritten as

$$Na \propto P_{peak} P_{average}$$

This relationship, in which Na is proportional to the product of P_{peak} and $P_{average}$, can be expected to hold true for both picosecond and femtosecond pulse light sources, as long as the peak power and average power are held constant. Our results demonstrate the utility of a picosecond pulse light source with high peak-power and high average power with low repetition rate for two-photon microscopy [11,13,18].

Actually, Konig's group previously reported that two-photon microscopy using a picosecond laser light source is much less harmful to living cells than a femtosecond laser [19]. Consistent with this, neither photo-bleaching nor photo-damage occurred during imaging of the hippocampal region, even at the maximum output power of the 1064-nm picosecond laser (500 mW). Damage to brain tissue at the focal point was observed in the cortical region when laser powers above 500 mW were applied in conjunction with a slow scanning speed (data not shown). These observations suggest that average power at 500 mW of our picosecond laser might represent the threshold for damage caused by absorption by water in the living brain. This higher threshold is consistent with the fact that the living brain continually removes heat through the circulation of cerebrospinal fluid and/or blood flow. In addition, our customized head chamber [Fig. 1(b)] contains a considerable amount of water as an immersion medium, and this could aid in diffusion of heat from the head. Such circulatory cooling action might permit *in vivo* two-photon imaging in live brains.

In the adult mouse, we could not always find the dentate gyrus granule cells, suggesting that developmental changes in light permeability in the mouse brain [10] influence the efficacy of two-photon excitation and acquisition of fluorescence images. Transmittance of visible and near-infrared light is higher in young animals and decreases over the course of development, suggesting that an age-dependent transmittance change might prevent visualization in older animals. In addition, operational state of the open-skull method also influence: for example, hemoglobin in blood cells absorbs light strongly even in the "biological window" of live organs. Thus, slight bleeding of the brain surface resulting from surgery might affect the transparency of tissue with respect to excitation and emission wavelengths.

Although we achieved a higher peak signal-to-background ratio in our imaging of the dendrites of hippocampal CA1 pyramidal neurons, it was not possible to identify the dendritic spine structure on neurons. The white matter and hippocampal alveus contained myelin that had a complex structure, as indicated by its higher refractive index and scattering. Because the laser spot size became larger due to aberrations resulting from the optical properties of the white matter and alveus, it might not have been possible to visualize the spine microstructure in the hippocampus. In addition, because of the method of line-scanning acquisition, motion due to the heartbeat might have accidentally obscured the fine structure. Scan speed during the imaging hippocampal area was 1/32 fps, and we guessed that an acquired image including dendritic spines might be technically difficult because the fine structure would move in reaction to the heartbeat on the timescale of a single scan.

4. Conclusion

Subsequent to previous work, we clearly demonstrate the feasibility of using a near-infrared picosecond high-power pulse laser for *in vivo* two-photon microscopy. In recent years, some femtosecond pulse lasers with wavelengths above 1000 nm and high output performance have become commercially available (e.g., FemtoTrain, Spirit, Spectra-Physics). The GSLD based light source was expected to provide stable operation for a longer period than a mode-locked laser. Furthermore, the introduction of a picosecond pulse laser to the microscope was not required negative chirp [11], and it might be sufficient to construct a two-photon microscope system that incorporates multiple lasers using a simple light guide optics. Application of the near-infrared high-peak power picosecond pulse laser would improve *in vivo* two-photon microscopy easily and become a powerful tool to visualize biological phenomena as synaptic conformation changes induced by synaptic plasticity in deeper region of brain. Visualization of all cortical regions and the hippocampus of the living mouse brain will help us to unravel the functions of neural circuits that express synaptic plasticity during learning and memory formation [20,21]. In the future, we hope that these techniques will contribute to fundamental technologies that could be used to reveal intact neural activities at the molecular and cellular levels in the hippocampal area and the basal ganglion and the functional connectome of the living brain.

Acknowledgments

We thank Dr. T. Hibi, Dr. K. Iijima and Dr. K. Otomo for helpful advice, and were also grateful for the technical assistance provided by Ms. E. Ito and Ms. M. Oguro of the Laboratory of Molecular and Cellular Biophysics in the Research Institute for Electronic Science, Hokkaido University. This study was supported by JSPS KAKENHI grants (No. 22113005 for TN, and RK, No. 26242082 for TN, SS and RK) of the Ministry of Education, Culture, Sports, Science and Technology (MEXT), Japan, by the Nano-Macro Materials, Devices and System Research Alliance (MEXT) (for TN, SS, and HY), and by the Network Joint Research Center for Materials and Devices (MEXT) (for TN, SS, and HY).